ACS Photonics

Article

pubs.acs.org/journal/apchd5

Maximizing Nonlinear Optical Conversion in Plasmonic Nanoparticles through Ideal Absorption of Light

Jérémy Butet,* Kuang-Yu Yang, Shourya Dutta-Gupta, and Olivier J. F. Martin

Nanophotonics and Metrology Laboratory (NAM), Swiss Federal Institute of Technology Lausanne (EPFL), 1015, Lausanne, Switzerland

ABSTRACT: The optimization of nonlinear optical processes in plasmonic structures is important for the design of efficient nonlinear nanosources of light. Considering the simple case of spherical nanoparticles, we clearly identify the most efficient channel for second-harmonic generation, thanks to physical insights provided by the generalized Mie theory. This channel corresponds to the excitation of electric dipolar modes at the fundamental wavelength and a quadrupolar second-harmonic emission. Interestingly, it is demonstrated that the second-harmonic generation intensity is directly related to the square of the absorbed power, which reproduces both the electric field enhancement and the specific size dependence of second-harmonic generation in the small-particle limit. Additionally, the absorbed power can be optimized by controlling the nanoparticle size. These results demonstrate that the optimization of the fundamental electric field is not sufficient for reaching the highest nonlinear conversion in plasmonic systems. The approach reported in this article proposes a new paradigm for the design of nonlinear plasmonic nanostructures, establishing new rules for the conception of efficient nonlinear plasmonic metamolecules on the basis of their linear response.

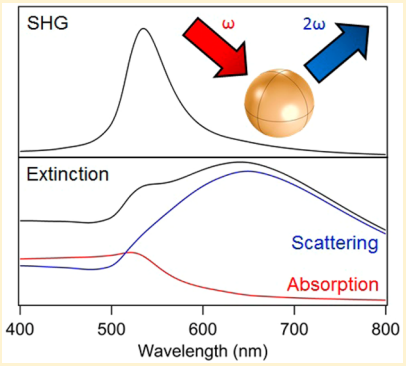

KEYWORDS: *plasmon, nonlinear optics, second-harmonic generation, Mie theory*

Over the past decade, a significant effort has been devoted to the observation of nonlinear optical processes in plasmonic nanostructures.[1] Indeed, nonlinear optical processes are effectively boosted by localized surface plasmon resonances, which induce strong near-field enhancement.[1,2] Among the different nonlinear optical processes, second-harmonic generation (SHG), whereby two photons at the fundamental frequency are converted into one at the second-harmonic (SH) frequency, is the simplest and probably the most studied nonlinear optical process in plasmonic systems.[2−13] The shape dependence of the SH intensity has been investigated for both centrosymmetric and non-centrosymmetric metallic nanostructures, addressing the related symmetry properties in great detail.[2−13] SHG from nanoparticle arrays and plasmonic metamaterials has also been extensively studied with the aim to control and design their nonlinear responses.[14−26] Several studies have reported the observation of SHG from single metallic nanostructures, paving the way for the design of practical applications such as nonlinear plasmonic sensing,[27] sensitive shape characterization,[28−30] and imaging.[31−33] However, it is important to increase the nonlinear conversion at the nanoscale for an optimal realization of these practical applications, and several approaches have been proposed to do so. Among those, Fano resonant nanostructures are appealing since they can increase the near-field localization of the incident light.[34−36] Indeed, since Fano resonances arise from the coupling between an optical bright mode and an optical dark mode, the engineering of these modes allows storing the electromagnetic energy in the weakly radiative dark mode, resulting in an increase of the near-field enhancement. Furthermore, it was recently shown that the combination of the intrinsic properties of Fano resonances and of SHG permits the design of nonlinear plasmonic nanorulers and nanosensors with very high sensitivities, beyond those achievable in the linear regime.[37,38] On the other hand, the enhancement of SHG in metal−dielectric nanodisks and split ring resonators was attributed to the excitation magnetic-like modes, highlighting further the influence on SHG of the coupling between the different plasmonic modes.[12,14,15,39,40] Finally, transferring the phase matching condition required for an efficient nonlinear conversion in nonlinear bulk crystals to the nanoscale has resulted in the development of double-resonant nanoantennas for an optimal SHG in plasmonic nanostructures.[34,35,41,42] These nanostructures exploit the fact that SHG is a nonlinear optical process involving two waves with distinct wavelengths, the fundamental wave and the SH wave, and that the electromagnetic properties of plasmonic systems can be independently optimized at these two wavelengths.

Relating the nonlinear conversion efficiency to easily computable physical quantities is essential for the design of efficient nonlinear nanosources of light. Considering the simplest plasmonic systems, i.e., gold and silver nanospheres, we unambiguously demonstrate in the small nanoparticle limit that the SH conversion is optimized when the absorption associated with the fundamental mode is maximized. The direct

Special Issue: Nonlinear and Ultrafast Nanophotonics

Received: January 15, 2016
Published: May 23, 2016

DOI: 10.1021/acsphotonics.6b00031
ACS Photonics 2016, 3, 1453−1460

consequence of this observation is that the maximization of the fundamental electric near-field only is not sufficient to reach the highest nonlinear conversion in plasmonic nanostructures. The direct comparison between linear and SH spectra emphasizes the importance of this observation for the extrapolation of the nonlinear response of plasmonic systems from their linear properties.

METHOD

Linear Mie Theory. Before discussing the SHG, let us briefly describe the linear optical properties of silver spherical nanoparticles. The extinction, scattering, and absorption of a 33 nm diameter silver nanoparticle in water have been calculated using the Mie theory and the multipolar expansion of the involved electromagnetic fields.[43] The dielectric constants for noble metals are taken from experimental data.[44] The extinction cross section C_{ext}, the scattering cross section C_{sca}, and absorption cross section C_{abs} are respectively given by

$$C_{ext} = \frac{2\pi}{k^2}\sum_{l=1}^{+\infty}(2l+1)\mathrm{Re}\{a_l + b_l\} \quad (1)$$

$$C_{sca} = \frac{2\pi}{k^2}\sum_{l=1}^{+\infty}(2l+1)[|a_l|^2 + |b_l|^2] \quad (2)$$

$$C_{abs} = C_{ext} - C_{sca} \quad (3)$$

where l is the mode order and k is the fundamental wavevector. These cross sections are shown for incident wavelengths ranging from 300 to 550 nm in Figure 1a, revealing a dipolar surface plasmon resonance at 394 nm. Note that the scattering cross section C_{sca} and absorption cross section C_{abs} are calculated considering only the dipolar mode ($l = 1$). The excitation of the quadrupolar surface plasmon resonance ($l = 2$) results in a small shoulder at 370 nm visible in the extinction spectrum.

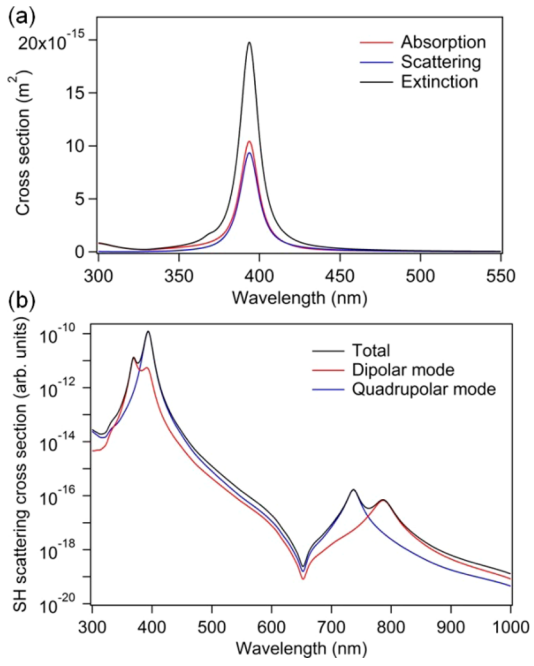

Figure 1. (a) Extinction cross section (black line), absorption cross section (red line), and scattering cross section (blue line) for a silver nanoparticle in water. The nanoparticle radius is 16.5 nm. (b) The corresponding SH scattering cross sections. The total SH cross section is shown in black. The contributions of the dipolar and quadrupolar SH emission modes are shown in red and blue, respectively.

Nonlinear Mie Theory. Now, we turn our attention to the second-order nonlinear optical response of the same 33 nm silver nanosphere and perform calculations using the Mie theory generalized to the case of surface SHG. The generalization of Mie theory to SHG has been discussed in several works.[45−47] Briefly, the fundamental electric fields are calculated using the classical Mie theory and then used to compute the nonlinear polarization oscillating at the second-harmonic frequency on the nanoparticle surface. To this end, the fundamental electric field is evaluated just below the interface, inside the metallic nanoparticle.[48] Without any loss of generality, only the component $\chi^{(2)}_{\perp\perp\perp}$ of the surface susceptibility tensor is considered here, where $\perp$ denotes the direction normal to the surface. This component is known to dominate the surface SH response for metallic nanoparticles.[49,50] Then, the nonlinear polarization can be written as

$$P_{surf,\perp}(2\omega) = \chi^{(2)}_{\perp\perp\perp} E_{\perp}(R^-, \omega)\, E_{\perp}(R^-, \omega)\, \delta(r - R^+) \quad (4)$$

where R is the nanoparticle radius. The multipolar development of the second-harmonic scattered field is obtained by applying the appropriate set of boundary conditions, considering the nonlinear polarization sheet at the interface between the nanoparticle and the surrounding medium.[51] In the case of the $\chi^{(2)}_{\perp\perp\perp}$ element, only transverse magnetic modes are excited since the nonlinear polarization sheet does not possess any tangential components. In this article, the dispersion of the nonlinear susceptibility is neglected and $\chi^{(2)}_{\perp\perp\perp}$ is then fixed to unity, since we are interested in comparing different plasmon enhancement of the nonlinear response. It should be noted that the electronic origin of SHG in plasmonic nanostructures has not been unambiguously determined so far. Although the hydrodynamic model considers that the nonlinearity arises from the motion of the conduction electrons only,[52−55] electronic transitions from the d-band to the conduction sp band may also contribute significantly to the nonlinear susceptibility as a consequence of the high density of states in the d-band.[56] Furthermore, the time-dependent density-functional approach has revealed that electronic surface states are able to enhance the SHG in metal.[57,58] The hydrodynamic model is the ideal framework to include the nonlocal effects and the nonlinear quantum tunneling occurring in nanostructures with very narrow gaps.[59,60] Although the discussion of these effects is not the scope of this study, they could be included in the present analysis through the choice of the nonlinear susceptibility. The total SH scattering cross section can be written as a superposition of modes:

$$C_{SHG} = \frac{c}{8\pi K_{SHG}^2}\sum_{l=1,m=0,\pm2}^{+\infty} |A_{l,m}^{E,SHG}|^2 \quad (5)$$

where $A_{l,m}^{E,SHG}(2\omega)$ are the coefficients calculated for the SH scattered wave and K_{SHG} is the wavevector of the SH wave. As in the linear regime, the contributions of the dipolar and quadrupolar modes to the total SH scattering cross section are calculated assuming $l = 1$ and $l = 2$, respectively. Only the dipolar and quadrupolar modes are considered here. The octupolar contribution, which has recently been observed for larger nanoparticles, still remains negligible for a nanoparticle diameter of 33 nm.[61,62]

DOI: 10.1021/acsphotonics.6b00031
ACS Photonics 2016, 3, 1453−1460

RESULTS AND DISCUSSION

SH Excitation Channels in Plasmonic Nanospheres. The SH cross-section is shown as a function of the fundamental wavelength in Figure 1b for a background refractive index n = 1.33 (water). The SHG spectrum reveals four surface plasmon resonances corresponding to the enhancement of the SH dipolar emission mode only (λ = 786 nm), the SH quadrupolar emission mode only (λ = 738 nm), and the enhancement of both (λ = 369 nm and λ = 393 nm). The most efficient mechanism leading to SH dipolar emission is the $E_1 + E_2 \rightarrow E_1$ mechanism, where the two terms on the left of the arrow refer to the nature of the interaction with the fundamental wave, and the third term describes the SH emission mode.[63] Hence, this notation describes here an SH dipolar emission (E_1) resulting from the combination of an electric dipole (E_1) and an electric quadrupole (E_2) excitation. The excitation channel including only dipolar modes ($E_1 + E_1 \rightarrow E_1$) is forbidden for centrosymmetric objects, like the spherical nanoparticle discussed in this work.[63] On the other hand, the SH quadrupolar emission mode can be excited without retardation effects at the fundamental frequency and arises from the $E_1 + E_1 \rightarrow E_2$ excitation channel. Indeed, the retardation effects are included in the quadrupolar nature of the SH emission, which results from the localization of the nonlinear sources over the entire nanoparticle surface. The resonances arising at the longest fundamental wavelength (λ = 738 and 786 nm, see Figure 1b) correspond to wavelengths for which the SH wavelengths match the quadrupolar and the dipolar surface plasmon resonance modes, respectively. Only the mode with symmetry properties identical to the surface plasmon resonance is enhanced; for example, the SH dipolar (quadrupolar) emission mode is enhanced when the SH wavelength is tuned close to the dipolar (quadrupolar) surface plasmon resonance. On the other hand, both dipolar and quadrupolar emission modes are enhanced for the resonances arising at the shortest wavelengths (350−425 nm, see Figure 1b). In these cases, the fundamental wavelength is close to the dipolar and quadrupolar resonances, and both SH emission modes benefit from the resulting high fundamental electric field. From Figure 1b, it is clear that the most efficient excitation channel is $E_1 + E_1 \rightarrow E_2$ when the incident wavelength matches the resonant wavelength of the dipolar surface plasmon mode, which results in an SH intensity 1 order of magnitude higher than the one given by the second most efficient channel, that is, $E_1 + E_2 \rightarrow E_1$. In the following, we will focus on the most efficient excitation channel ($E_1 + E_1 \rightarrow E_2$) and discuss the parameters influencing the enhancement of the nonlinear response.

SHG in Silver Nanoparticles. Figure 2a shows the maximal SHG for a silver nanoparticle in water and in a glass matrix as a function of its radius R. For the two embedding media, the SHG reaches a maximum value for intermediate nanoparticle sizes: R = 16.5 nm for a silver nanoparticle in water and R = 15.5 nm for a glass matrix (n = 1.5). This observation demonstrates that in this range the SHG does not monotonously increase or decrease with the nanoparticle size and that the nanoparticle dimension must be optimized for reaching the highest nonlinear conversion. Neglecting the plasmonic enhancement at the SH wavelength, the scattered SH power from a single spherical nanoparticle can be rewritten, in the small-nanoparticle limit, as[63]

$$P_{SHG} \approx G|\chi^2{}_{\perp\perp\perp}|^2|E_\perp(R^-, \omega)|^4(kR)^6 \quad (7)$$

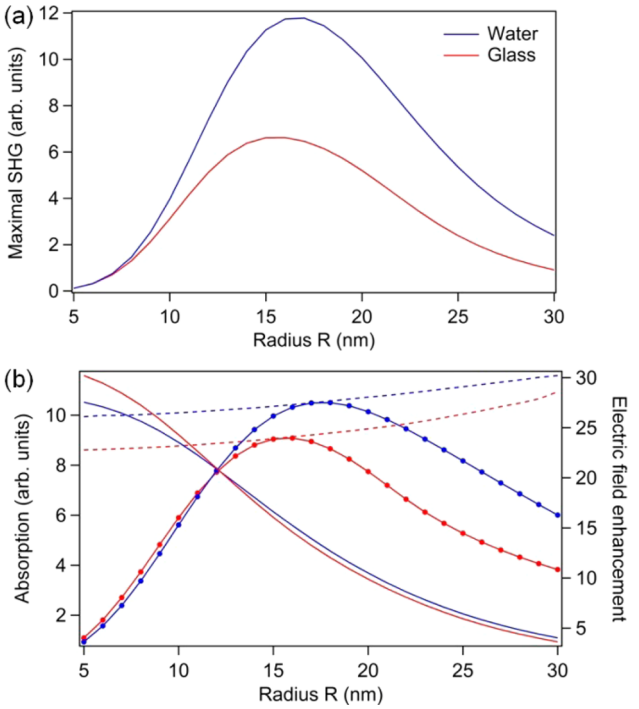

Figure 2. (a) Maximal SHG (defined as the maximum of the SH scattering cross section observed in the corresponding spectrum) as a function of the nanoparticle radius R. (b) Absorption in a silver nanoparticle as a function of its radius R (dots linked by a continuous line, left axis), the maximal absorption given by eq 12 (dashed lines, left axis), and the electric field enhancement evaluated at the center of the nanoparticle (continuous lines, right axis). The nanoparticle is either in water (blue lines) or in a glass matrix (red lines).

where G is a constant.

As expected, the scattered SH power increases nonlinearly with the fundamental electric field as shown by the third term in eq 7. The fundamental electric field has been calculated at the nanoparticle center, Figure 2b. In the dipolar approximation, the electric field is homogeneous inside the nanoparticle and the electric field at the particle center is a good representation for its value. The internal electric field is higher for small nanoparticles. From this observation, one can expect that SHG is higher for small nanoparticles. However, neglecting all resonant effects, the dipolar and quadrupolar emission modes have the same dependence with the scattering parameter $x = kR$, where R is the nanosphere radius and k the fundamental wavevector. Both SH modes scale with an x^6 dependence due to the need of retardation effects. As a consequence, the best case for high nonlinear conversion is a compromise between electric field enhancement and retardation effects.

Relation between SHG and Absorption. For a systematic optimization of SHG in plasmonic nanoparticles, it is particularly useful to relate the best nanoparticle size to a physical quantity, the computation of which is straightforward and fast. For this purpose, the maximal absorption was computed and shown as a function of the nanoparticle radius; see Figure 2b. Interestingly, the highest absorption is reached for a nanoparticle radius R = 16.5 nm when the nanoparticle is in water and for R = 15.5 nm when the nanoparticle is embedded in a glass matrix. These values are exactly identical to those obtained for the maximal SHG, giving a first hint that absorption at the fundamental wavelength could be used as an

DOI: 10.1021/acsphotonics.6b00031
ACS Photonics 2016, 3, 1453−1460

indicator to reach the highest SHG enhancement factor. The absorption cross section can be rewritten as

$$C_{abs} = \frac{P_{abs}}{I_i} \tag{8}$$

where I_i is the incident intensity and P_{abs} is the absorbed power. For ohmic losses, the absorbed power P_{abs} is given by the following formula:[64]

$$P_{abs} = \frac{1}{2}\int_{\Omega} dV\ \mathrm{Re}\{\sigma\}|\mathbf{E}(\mathbf{r})|^2 \tag{9}$$

where the integration is performed over the volume of the nanoparticle. The conductivity σ is expressed as

$$\sigma = -i\omega\varepsilon_0(\varepsilon_r - 1) \tag{10}$$

From eq 9, the relation between absorption at the excitation wavelength and SHG enhancement is obvious. Taking the square of eq 9, one finds the adequate size dependence (R^6) and field enhancement ($|\mathbf{E}|^4$), and therefore P_{SHG} is proportional to $(P_{abs})^2$. The competition between the size dependence and the field enhancement explains why the maximal SHG is not reached when the fundamental near-field is maximized, i.e., for small nanoparticles; see Figure 2b. Furthermore, it should be emphasized that the competition between size dependence and field enhancement results in an optimal nanoparticle radius (R = 16.5 nm for a silver nanoparticle in water and R = 15.5 nm for a silver nanoparticle embedded in a glass matrix). Note that the frequency/wavelength dependence is underestimated in this relation (ω^2 instead of ω^6), but the surface plasmon resonance shift is small in the considered size range, resulting in a weak influence on the SHG. At this point, it is worth mentioning that, due to the requirement for a high electric field enhancement inside the nanoparticle to reach a consequent nonlinear conversion, several groups have recently proposed to use dielectric nanoparticles, instead of plasmonic ones, for the observation of nonlinear optical processes at the nanoscale.[65−67]

Optimization of SHG through Ideal Absorption of Light. Now that the relation between maximal absorption and maximal SHG has been established, it is worthwhile discussing the conditions under which absorption in nanoparticles can be optimized. This problem has been widely addressed by the antenna community.[68,69] The maximal absorption for a given antenna mode is reached when the amount of absorbed energy equals the amount of the scattered one, i.e., when the following relation is satisfied:

$$C_{abs,l} = C_{sca,l} = \frac{C_{ext,l}}{2} \tag{11}$$

In the case of Mie theory, the maximal absorption for the mode of order l is given by[70,71]

$$C_{abs,l}^{max} = \frac{2l+1}{8\pi}\lambda^2 \tag{12}$$

The maximal absorption is plotted in dashed lines in Figure 2b. One can observe that the absorption reaches its maximal value when the sphere radius is R = 16.5 nm for a silver nanoparticle in water and R = 15.5 nm for a silver nanoparticle embedded in a glass matrix. Looking at Figure 1a, it is obvious that the relation $C_{abs,l} \approx C_{sca,l}$ stands in the latter case. These results demonstrate that computing the absorption is an excellent technique for optimizing SHG in plasmonic systems.

Case of Gold Nanoparticles. In order to further confirm the validity of this approach, the case of nanoparticles made of gold, which is also a metal widely used in plasmonics, is considered in the following. Figure 3a shows the extinction,

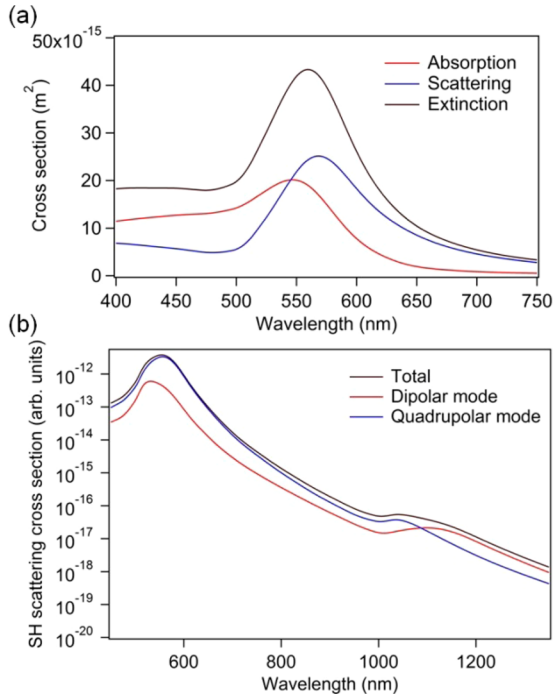

Figure 3. (a) Extinction cross section (black line), absorption cross section (red line), and scattering cross section (blue line) of a gold nanoparticle in water. The nanoparticle radius is 45 nm. (b) Corresponding SH scattering cross sections. The total SH cross section is shown in black. The contributions of the dipolar and quadrupolar SH emission modes are shown in red and blue, respectively.

absorption, and scattering spectra for a 45 nm gold nanoparticle in water. A strong dipolar surface plasmon resonance is observed for an incident wavelength close to 560 nm. As in the case of the silver nanoparticle discussed previously, the SHG spectrum reveals four resonances corresponding to the plasmonic enhancement of the nonlinear response at either the fundamental or SH wavelengths; see Figure 3b. The most efficient excitation channel is again $E_1 + E_1 \rightarrow E_2$ when the fundamental wavelength matches the dipolar surface plasmon resonance, Figure 4a. Since the dipolar surface plasmon resonance arises at different wavelength in gold and silver nanoparticles, one expects that the nanoparticle dimension giving the highest SHG is not the same. This is indeed the case: the optimal sphere radius is R = 46 nm for a gold nanoparticle in water and R = 38 nm for a gold nanoparticle embedded in a glass matrix. The comparison with the absorption and its maximal value given by eq 12 indicates that these sizes correspond indeed to that with ideal absorption.

Relation between the Linear Spectra and the SH Spectrum. As discussed in the Introduction, the determination of specific rules for an efficient design of nonlinear plasmonic metamolecules is mandatory for the development of new applications. In this context, the validity of Miller's rules[72] for the description of nonlinear plasmonic systems has been investigated by several groups.[23,73,74] In a few words, Miller's rule expresses the fact that, in piezoelectric crystals, the ratio

DOI: 10.1021/acsphotonics.6b00031
ACS Photonics 2016, 3, 1453−1460

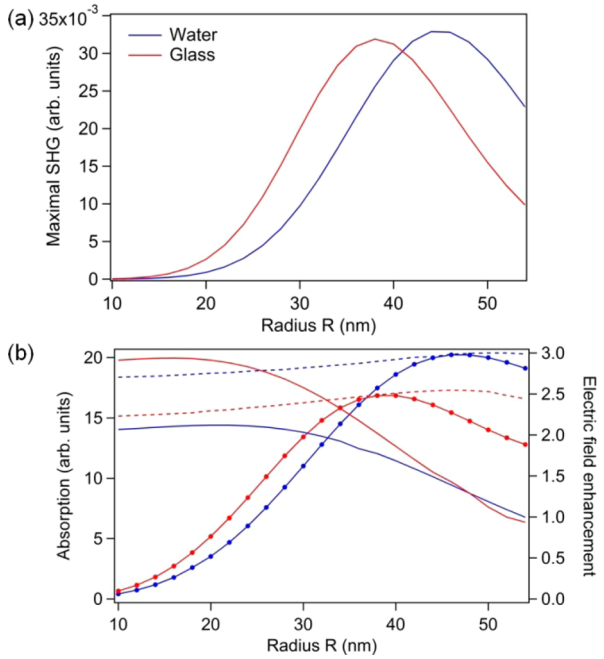

Figure 4. (a) Maximal SHG (defined as the maximum of the SH scattering cross section observed in the corresponding spectrum) as a function of the nanoparticle radius *R*. (b) Absorption in a gold nanoparticle as a function of its radius *R* (dots linked by a continuous line, left axis), the maximal absorption given by eq 12 (dashed lines, left axis), and the electric field enhancement evaluated at the center of the nanoparticle (continuous lines, right axis). The nanoparticle is either in water (blue lines) or in a glass matrix (red lines).

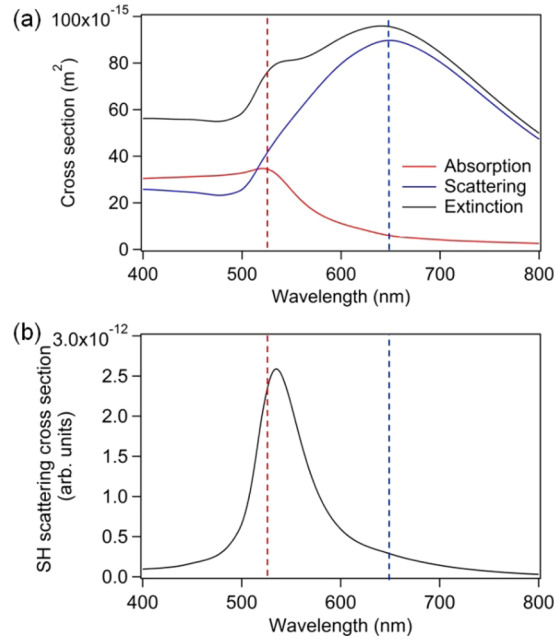

Figure 5. (a) Extinction cross section (black line), absorption cross section (red line), and scattering cross section (blue line) of a gold nanoparticle in water. The nanoparticle radius is 75 nm. (b) Corresponding total SH scattering cross section. The red and blue dashed lines show the maximal absorption and scattering, respectively.

between the nonlinear susceptibility and the product of the linear susceptibility of the same material at the pump and generated wavelengths is almost constant as described by the anharmonic oscillator model.[75] In the field of plasmonics, several attempts have been made to relate the nonlinear conversion yield of a given plasmonic system to its linear far-field properties (scattering or reflectance) at both the fundamental and generated wavelengths.[23,73,74] As a few successes for this approach, we can note that the anharmonic oscillator model has been applied for understanding the third-order nonlinear response, i.e., the third-harmonic generation (THG), for plasmonic nanoantennas[76] and metamolecules supporting Fano resonances.[74] In the case of SHG, Miller's rule is not always fulfilled and seems to stand only for plasmonic nanostructures resonant at the SH wavelength only, with no resonant behavior at the fundamental wavelength,[23,73,74] and for nanoantennas with non-centrosymmetric shapes.[77] In light of the results discussed previously, the discrepancy of Miller's rule in specific cases is explained by the fact that SHG is optimized when the absorption is maximal, not the scattering; see Figure 5. The slight wavelength shift between the maximal SHG and the maximal absorption is explained by the contribution of high-order modes in these two processes. It should be emphasized that, for a given resonance, there is a small shift between the scattering and the absorption peaks as revealed by the damped oscillator model.[78] Even more important in the present context, the ratio between the radiative and intrinsic losses associated with a given resonance depends on the mode order *l*. The results shown in Figure 5 demonstrate that SHG is optimized by the presence of absorptive plasmonic modes at the fundamental wavelength. Indeed, SHG for an incident wavelength λ = 650 nm is relatively weak despite a strong linear scattering at this wavelength. Furthermore, it should be noted that a strong absorption induced by a high imaginary part of the dielectric constant of gold, as observed at wavelengths shorter than ~500 nm, does not induce a significant SH intensity.

Toward the Optimization of the SHG in Complex Plasmonic Systems. Having so far focused on the SHG from spherical nanoparticles, let us say a few words about the optimization of the SHG in complex plasmonic systems, as those supporting Fano resonances.[79,80] As an example, we now consider a gold nanodolmen composed of three nanorods with dimensions 120 nm × 40 nm × 40 nm. The nanorods are organized as shown in the inset of Figure 6a. It was previously reported that the optical response of such a plasmonic dolmen exhibits a Fano resonance, which results from the interaction between a dipolar bright mode supported by the top nanorod and a quadrupolar dark mode supported by the two parallel nanorods.[81,82] Due to their complex shapes, the optical response of gold dolmens cannot be computed in the framework of the Mie theory, and a surface integral equation method was used instead.[83,84] The scattering, the absorption in the top nanorod, and the absorption in the two parallel nanorods are shown in Figure 6a. Interestingly, asymmetric Fano profiles are observed in the three spectra, as well as in the SHG spectrum, Figure 6b. However, the maximal SHG arises at a wavelength away from the Fano resonance, at 520 nm. This wavelength is close to a maximum of the absorption in the two parallel nanorods, while the absorption in the top nanorod evolves very slowly in this spectral range, giving a clear indication that the SHG enhancement occurs in the two parallel nanorods and not in the top nanorod. This result points out the potential of the method proposed in this article for the analysis of the SHG from coupled plasmonic nanostructures and its optimization, enabling identifying which nanoparticle of a

DOI: 10.1021/acsphotonics.6b00031
ACS Photonics 2016, 3, 1453−1460

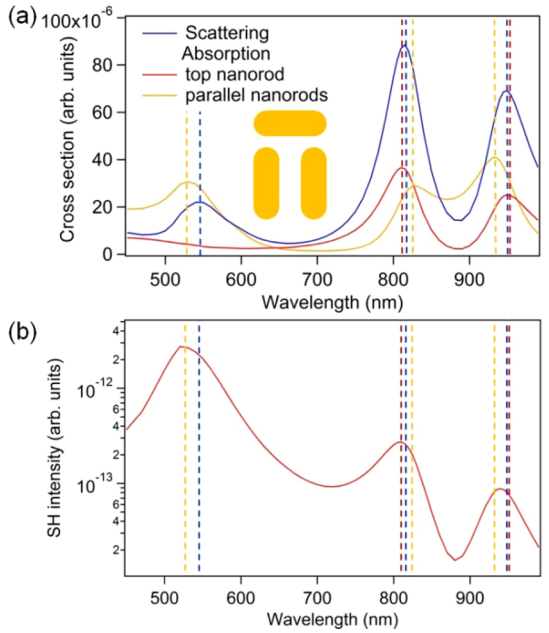

Figure 6. (a) Scattering (blue line), absorption in the top nanorod (red line), and absorption in the parallel nanorods (orange line) for a gold dolmen in glass. The nanorod size is 120 nm × 40 nm × 40 nm. The distance between the two parallel nanorods is 40 nm. The distance between the top nanorod and the two parallel ones is 20 nm. (b) Corresponding total SH intensity. The dashed lines indicate the maximal absorption in the top nanorod, the maximal absorption in the parallel nanorods, and the maximal scattering.

coupled plasmonic system contributes to the enhancement of the SHG.

CONCLUSIONS

In conclusion, the optimization of the SHG in plasmonic nanosystems has been discussed in the simple case of spherical nanoparticles. Thanks to physical insights provided by the Mie theory generalized to SHG, we clearly identified the most efficient channel giving the highest nonlinear conversion. This channel corresponds to the excitation of electric dipolar modes at the fundamental wavelength and a quadrupolar SH emission. We showed that the SHG intensity is related to the square of the absorbed power, which reproduces both the electric field enhancement and the size dependence of SHG. Interestingly, the absorbed power can be optimized by controlling the nanoparticle size. These results demonstrate that the optimization of the fundamental electric field is not sufficient for reaching the highest nonlinear conversion in plasmonic systems. This observation is particularly relevant for the optimization of the output signal of nonlinear plasmonic sensors, as well as for their exact calibration.[37,38,85] The approach reported in this article proposes a new paradigm for the design of complex nonlinear metamolecules, as the ones supporting Fano resonances,[35] and metamaterials[14−26] based on the control of the intrinsic (ohmic) losses[86,87] and can be extended to other nonlinear optical processes, as THG[74,76,88] and multiphoton photoluminescence.[89,90]

AUTHOR INFORMATION

Corresponding Author

*E-mail: jeremy.butet@epfl.ch.

Notes

The authors declare no competing financial interest.

ACKNOWLEDGMENTS

Funding from the Swiss National Science Foundation is gratefully acknowledged (projects 200020_153662 and CR23I2_147279).

REFERENCES

(1) Kauranen, M.; Zayats, A. V. Nonlinear Plasmonics. *Nat. Photonics* **2012**, *6*, 737−748.
(2) Butet, J.; Brevet, P.-F.; Martin, O. J. F. Optical Second Harmonic Generation in Plasmonic Nanostructures: From Fundamental Principles to Advanced Applications. *ACS Nano* **2015**, *9*, 10545−10562.
(3) Bouhelier, A.; Beversluis, M.; Hartschuch, A.; Novotny, L. Near-Field Second-Harmonic Generation Induced by Local Field Enhancement. *Phys. Rev. Lett.* **2003**, *90*, 013903.
(4) Bozhevolnyi, S. I.; Beermann, J.; Coello, V. Direct Observation of Localized Second-Harmonic Enhancement in Random Metal Nanostructures. *Phys. Rev. Lett.* **2003**, *90*, 197403.
(5) Jin, R.; Jureller, J. E.; Kim, H. Y.; Scherer, N. F. Correlating Second Harmonic Optical Responses of Single Ag Nanoparticles with Morphology. *J. Am. Chem. Soc.* **2005**, *127*, 12482.
(6) van Nieuwstadt, J. A. H.; Sandtke, M.; Harmsen, R. H.; Segerink, F. B.; Prangsma, J. C.; Enoch, S.; Kuipers, L. Strong Modification of the Nonlinear Optical Response of Metallic Subwavelength Hole Arrays. *Phys. Rev. Lett.* **2006**, *97*, 146102.
(7) Valev, V. K.; Silhanek, A. V.; Verellen, N.; Gillijns, W.; Van Dorpe, P.; Aktsipetrov, O. A.; Vandenbosch, G. A. E.; Moshchalkov, V. V.; Verbiest, T. Asymmetric Optical Second-Harmonic Generation from Chiral G-Shaped Gold Nanostructures. *Phys. Rev. Lett.* **2010**, *104*, 127401.
(8) Butet, J.; Duboisset, J.; Bachelier, G.; Russier-Antoine, I.; Benichou, E.; Jonin, C.; Brevet, P.-F. Optical Second Harmonic Generation of Single Metallic Nanoparticles Embedded in a Homogeneous Medium. *Nano Lett.* **2010**, *10*, 1717−1721.
(9) Zhang, Y.; Grady, N. K.; Ayala-Orozco, C.; Halas, N. J. Three-Dimensional Nanostructures as Highly Efficient Generators of Second Harmonic Light. *Nano Lett.* **2011**, *11*, 5519−5523.
(10) Hasan, S.-B.; Etrich, C.; Filter, R.; Rockstuhl, C.; Lederer, F. Enhancing the Nonlinear Response of Plasmonic Nanowire Antennas by Engineering their Terminations. *Phys. Rev. B: Condens. Matter Mater. Phys.* **2013**, *88*, 205125.
(11) Reichenbach, P.; Horneber, A.; Gollmer, D. A.; Hille, A.; Mihaljevic, J.; Schäfer, C.; Kern, D. P.; Meixner, A. J.; Zhang, D.; Fleischer, M.; Eng, L. M. Nonlinear Optical Point Light Sources through Field Enhancement at Metallic Nanocones. *Opt. Express* **2014**, *22*, 15484−15501.
(12) Kruk, S.; Weismann, M.; Bykov, A. Y.; Mamonov, E. A.; Kolmychek, I. A.; Murzina, T.; Panoiu, N. C.; Neshev, D. N.; Kivshar, Y. S. Enhanced Magnetic Second-Harmonic Generation from Resonant Metasurfaces. *ACS Photonics* **2015**, *2*, 1007−1012.
(13) de Ceglia, D.; Vincenti, M. A.; de Angelis, C.; Locatelli, A.; Haus, J. W.; Scalora, M. Role of Antenna Modes and Field Enhancement in Second Harmonic Generation from Dipole Nanoantenna. *Opt. Express* **2015**, *23*, 1715−1729.
(14) Husu, H.; Siikanen, R.; Mäkitalo, J.; Lehtolahti, J.; Laukkanen, J.; Kuittinen, M.; Kauranen, M. Metamaterials with Tailored Nonlinear Optical Response. *Nano Lett.* **2012**, *12*, 673−677.
(15) Linden, S.; Niesler, F. B. P.; Förstner, J.; Grynko, Y.; Meier, T.; Wegener, M. Collective Effects in Second-Harmonic Generation from Split-Ring-Resonator Arrays. *Phys. Rev. Lett.* **2012**, *109*, 015502.
(16) Czaplicki, R.; Husu, H.; Siikanen, R.; Mäkitalo, J.; Kauranen, M. Enhancement of Second-Harmonic Generation from Metal Nanoparticles by Passive Elements. *Phys. Rev. Lett.* **2013**, *110*, 093902.
(17) Konishi, K.; Higuchi, T.; Li, J.; Larsson, J.; Ishii, S.; Kuwata-Gonokami, M. Polarization-Controlled Circular Second-Harmonic

DOI: 10.1021/acsphotonics.6b00031
ACS Photonics 2016, 3, 1453−1460

Generation from Metal Hole Arrays with Threefold Rotational Symmetry. *Phys. Rev. Lett.* **2014**, *112*, 135502.
(18) Chen, P.-Y.; Argyropoulos, C.; D'Aguanno, G.; Alù, A. Enhanced Second-Harmonic Generation by Metasurface Nanomixer and Nanocavity. *ACS Photonics* **2015**, *2*, 1000−1006.
(19) Kolkowski, R.; Petti, L.; Rippa, M.; Lafargue, C.; Zyss, J. Octupolar Plasmonic Meta-Molecules for Nonlinear Chiral Watermarking at Subwavelength Scale. *ACS Photonics* **2015**, *2*, 899−906.
(20) Minovich, A. E.; Miroshnichenko, A. E.; Bykov, A. Y.; Murzina, T. V.; Neshev, D. N.; Kivshar, Y. S. Functional and Nonlinear Optical Metasurfaces. *Laser Phot. Rev.* **2015**, *9*, 195−213.
(21) Segal, N.; Keren-Zur, S.; Hendler, N.; Ellenbogen, T. Controlling Light with Metamaterials-Based Nonlinear Photonic Crystals. *Nat. Photonics* **2015**, *9*, 180−184.
(22) Li, G.; Chen, S.; Pholchai, N.; Reineke, B.; Wong, P. W. H.; Pun, E. Y. B.; Cheah, K. W.; Zentgraf, T.; Zhang, S. Continuous Control of the Nonlinearity Phase for Harmonic Generations. *Nat. Mater.* **2015**, *14*, 607−612.
(23) O'Brien, K.; Suchowski, H.; Rho, J.; Salandrino, A.; Boubacar, K.; Yin, X.; Zhang, X. Predicting Nonlinear Properties of Metamaterials from the Linear Response. *Nat. Mater.* **2015**, *14*, 379−383.
(24) Metzger, B.; Gui, L.; Fuchs, J.; Floess, D.; Hentschel, M.; Giessen, H. Strong Enhancement of Second Harmonic Emission by Plasmonic Resonances at the Second Harmonic Wavelength. *Nano Lett.* **2015**, *15*, 3917−3922.
(25) Black, L.-J.; Wiecha, P. R.; Wang, Y.; de Groot, C. H.; Paillard, V.; Girard, C.; Muskens, O. L.; Arbouet, A. Tailoring Second Harmonic Generation in Single L-Shaped Plasmonic Nanoantennas from the Capacitive to Conductive Coupling Regime. *ACS Photonics* **2015**, *2*, 1592−1601.
(26) Keren-Zur, S.; Avayu, O.; Michaeli, L.; Ellenbogen, T. Nonlinear Beam Shaping with Plasmonic Metasurfaces. *ACS Photonics* **2016**, *3*, 117−123.
(27) Butet, J.; Russier-Antoine, I.; Jonin, C.; Lascoux, N.; Benichou, E.; Brevet, P.-F. Sensing with Multipolar Second Harmonic Generation from Spherical Metallic Nanoparticles. *Nano Lett.* **2012**, *12*, 1697−1701.
(28) Bautista, G.; Huttunen, M. J.; Mäkitalo, J.; Kontio, J. M.; Simonen, J.; Kauranen, M. Second-Harmonic Generation Imaging of Metal Nano-Objects with Cylindrical Vector Beams. *Nano Lett.* **2012**, *12*, 3207−3212.
(29) Butet, J.; Thyagarajan, K.; Martin, O. J. F. Ultrasensitive Optical Shape Characterization of Gold Nanoantennas Using Second Harmonic Generation. *Nano Lett.* **2013**, *13*, 1787−1792.
(30) Sauerbeck, C.; Haderlein, M.; Schürer, B.; Braunschweig, B.; Peukert, W.; Taylor, R. N. K. Shedding Light on the Growth of Gold Nanoshells. *ACS Nano* **2014**, *8*, 3088−3096.
(31) Valev, V. K.; Volodin, A.; Silhanek, A. V.; Gillijns, W.; De Clercq, B.; Jeyaram, Y.; Paddubrouskaya, H.; Biris, C. G.; Panoiu, N. C.; Aktsipetrov, O. A.; Moshchalkov, V. V.; Verbiest, T. Plasmons Reveal the Direction of Magnetization in Nickel Nanostructures. *ACS Nano* **2011**, *5*, 91−96.
(32) Valev, V. K. Characterization of Nanostructured Plasmonic Surfaces with Second Harmonic Generation. *Langmuir* **2012**, *28*, 15454−15471.
(33) Biswas, S.; Liu, X.; Jarrett, J. W.; Brown, D.; Pustovit, V.; Urbas, A.; Knappenberger Jr, K. L.; Nealey, P. F.; Vaia, R. A. Nonlinear Chiro-Optical Amplification by Plasmonic Nanolens Arrays Formed via Directed Assembly of Gold Nanoparticles. *Nano Lett.* **2015**, *15*, 1836−1842.
(34) Thyagarajan, K.; Rivier, S.; Lovera, A.; Martin, O. J. F. Enhanced Second-Harmonic Generation from Double Resonant Plasmonic Antennae. *Opt. Express* **2012**, *20*, 12860−12865.
(35) Thyagarajan, K.; Butet, J.; Martin, O. J. F. Augmenting Second Harmonic Generation Using Fano Resonances in Plasmonic Systems. *Nano Lett.* **2013**, *13*, 1847−1851.
(36) Zhang, Y.; Wen, F.; Zhen, Y. R.; Nordlander, P.; Halas, N. J. Coherent Fano Resonances in a Plasmonic Nanocluster Enhance Optical Four-Wave Mixing. *Proc. Natl. Acad. Sci. U. S. A.* **2013**, *110*, 9215−9219.
(37) Butet, J.; Martin, O. J. F. Nonlinear Plasmonic Nanorulers. *ACS Nano* **2014**, *8*, 4931−4939.
(38) Butet, J.; Martin, O. J. F. Refractive Index Sensing with Fano Resonant Plasmonic Nanostructures: A Symmetry Based Nonlinear Approach. *Nanoscale* **2014**, *6*, 15262−15270.
(39) Klein, M. W.; Enkrich, C.; Wegener, M.; Linden, S. Second-Harmonic Generation from Magnetic Metamaterials. *Science* **2006**, *313*, 502−504.
(40) Ciracì, C.; Poutrina, E.; Scalora, M.; Smith, D. R. Origin of second-harmonic generation enhancement in optical split-ring resonators. *Phys. Rev. B: Condens. Matter Mater. Phys.* **2012**, *85*, 201403.
(41) Aouani, H.; Navarro-Cia, M.; Rahmani, M.; Sidiropoulos, T. P. H.; Hong, M.; Oulton, R. F.; Maier, S. A. Multiresonant Broadband Optical Antennas As Efficient Tunable Nanosources of Second Harmonic Light. *Nano Lett.* **2012**, *12*, 4997−5002.
(42) Celebrano, M.; Wu, X.; Baselli, M.; Großmann, S.; Biagioni, P.; Locatelli, A.; De Angelis, C.; Cerullo, G.; Osellame, R.; Hecht, B.; Duò, L.; Ciccacci, F.; Finazzi, M. Mode Matching in Multiresonant Plasmonic Nanoantennas for Enhanced Second Harmonic Generation. *Nat. Nanotechnol.* **2015**, *10*, 412−417.
(43) Bohren, C. F.; Huffman, D. R. *Absorption and Scattering of Light by Small Particles*; Wiley: New York, 1983.
(44) Johnson, P. B.; Christy, R. W. Optical Constants of the Noble Metals. *Phys. Rev. B* **1972**, *6*, 4370−4379.
(45) Östling, D.; Stampfli, P.; Benneman, K. H. Theory of Nonlinear Optical Properties of Small Metallic Spheres. *Z. Phys. D: At., Mol. Clusters* **1993**, *28*, 169−175.
(46) Pavlyukh, Y.; Hubner, W. Nonlinear Mie Scattering from Spherical Particles. *Phys. Rev. B: Condens. Matter Mater. Phys.* **2004**, *70*, 245434.
(47) Gonella, G.; Dai, H.-L. Determination of Adsorption Geometry on Spherical Particles from Nonlinear Mie Theory Analysis of Surface Second Harmonic Generation. *Phys. Rev. B: Condens. Matter Mater. Phys.* **2011**, *84*, 121402.
(48) Sipe, J. E.; So, V. C. Y.; Fukui, M.; Stegeman, G. I. Analysis of Second-Harmonic Generation at Metal Surfaces. *Phys. Rev. B: Condens. Matter Mater. Phys.* **1980**, *21*, 4389.
(49) Bachelier, G.; Butet, J.; Russier-Antoine, I.; Jonin, C.; Benichou, E.; Brevet, P.-F. Origin of Optical Second-Harmonic Generation in Spherical Gold Nanoparticles: Local Surface and Nonlocal Bulk Contributions. *Phys. Rev. B: Condens. Matter Mater. Phys.* **2010**, *82*, 235403.
(50) Wang, F. X.; Rodriguez, F. J.; Albers, W. M.; Ahorinta, R.; Sipe, J. E.; Kauranen, M. Surface and Bulk Contributions to the Second-Order Nonlinear Optical Response of a Gold Film. *Phys. Rev. B: Condens. Matter Mater. Phys.* **2009**, *80*, 233402.
(51) Heinz, T. F. In *Nonlinear Surface Electromagnetic Phenomena*; Elsevier: Amsterdam, 1991; pp 353−415.
(52) Rudnick, J.; Stern, E. A. Second-Harmonic Radiation from Metal Surfaces. *Phys. Rev. B* **1971**, *4*, 4274.
(53) Scalora, M.; Vincenti, M. A.; de Ceglia, D.; Roppo, V.; Centini, M.; Akozbek, N.; Bloemer, M. J. Second- and Third-Harmonic Generation in Metal-Based Structures. *Phys. Rev. A: At., Mol., Opt. Phys.* **2010**, *82*, 043828.
(54) Ciracì, C.; Poutrina, E.; Scalora, M.; Smith, D. R. Second-Harmonic Generation in Metallic Nanoparticles: Clarification of the Role of the Surface. *Phys. Rev. B: Condens. Matter Mater. Phys.* **2012**, *86*, 115451.
(55) Ginzburg, P.; Krasavin, A. V.; Wurtz, G. A.; Zayats, A. V. Nonperturbative Hydrodynamic Model for Multiple Harmonics Generation in Metallic Nanostructures. *ACS Photonics* **2015**, *2*, 8−13.
(56) Luce, T. A.; Hubner, W.; Bennemann, K. H. Theory for the Nonlinear Optical Response at Noble-Metal Surfaces with Non-equilibrium Electrons. *Z. Phys. B: Condens. Matter* **1997**, *102*, 223−232.

DOI: 10.1021/acsphotonics.6b00031
ACS Photonics 2016, 3, 1453−1460

(57) Liebsch, A. Second-Harmonic Generation at Simple Metal Surfaces. *Phys. Rev. Lett.* **1988**, *61*, 1233.
(58) Schaich, W. L. Calculations of Second-Harmonic Generation for a Jellium Metal Surface. *Phys. Rev. B: Condens. Matter Mater. Phys.* **2000**, *61*, 10478.
(59) Scalora, M.; Vincenti, M. A.; de Ceglia, D.; Haus, J. W. Nonlocal and Quantum-Tunneling Contributions to Harmonic Generation in Nanostructures: Electron-Cloud-Screening Effects. *Phys. Rev. A: At., Mol., Opt. Phys.* **2014**, *90*, 013831.
(60) Haus, J. W.; de Ceglia, D.; Vincenti, M. A.; Scalora, M. Nonlinear Quantum Tunneling Effects in Nanoplasmonic Environments: Two-Photon Absorption and Harmonic Generation. *J. Opt. Soc. Am. B* **2014**, *31*, A13−A19.
(61) Butet, J.; Bachelier, G.; Russier-Antoine, I.; Jonin, C.; Benichou, E.; Brevet, P.-F. Interference between Selected Dipoles and Octupoles in the Optical Second-Harmonic Generation from Spherical Gold Nanoparticles. *Phys. Rev. Lett.* **2010**, *105*, 077401.
(62) Capretti, A.; Pecora, E. F.; Forestiere, C.; Dal Negro, L.; Miano, G. Size-Dependent Second-Harmonic Generation from Gold Nanoparticles. *Phys. Rev. B: Condens. Matter Mater. Phys.* **2014**, *89*, 125414.
(63) Dadap, J. I.; Shan, J.; Eisenthal, K. B.; Heinz, T. F. Second-Harmonic Rayleigh Scattering from a Sphere of Centrosymmetric Material. *Phys. Rev. Lett.* **1999**, *83*, 4045−4048.
(64) Shcherbakov, M. R.; Neshev, D. N.; Hopkins, B.; Shorokhov, A. S.; Staude, I.; Melik-Gaykazyan, E. V.; Decker, M.; Ezhov, A. A.; Miroshnichenkov, A. E.; Brener, I.; Fedyanin, A. A.; Kivshar, Y. S. Enhanced Third-Harmonic Generation in Silicon Nanoparticles Driven by Magnetic Response. *Nano Lett.* **2014**, *14*, 6488−6492.
(65) Yang, Y.; Wang, W.; Boulesbaa, A.; Kravchenko, I. I.; Briggs, D. P.; Puretzky, A.; Geohegan, A.; Valentine, J. Nonlinear Fano-Resonant Dielectric Metasurfaces. *Nano Lett.* **2015**, *15*, 7388−7393.
(66) Shcherbakov, M. R.; Vabishchevich, P. P.; Shorokhov, A. S.; Chong, K. E.; Choi, D. Y.; Staude, I.; Miroshnichenko, A. E.; Neshev, D. N.; Fedyanin, A. A.; Kivshar, Y. S. Ultrafast All-Optical Switching with Magnetic Resonances in Nonlinear Dielectric Nanostructures. *Nano Lett.* **2015**, *15*, 6985−6990.
(67) Kern, A. M.; Martin, O. J. F. Pitfalls in the Determination of Optical Cross Sections from Surface Integral Equation Simulations. *IEEE Trans. Antennas Propag.* **2010**, *58*, 2158−2161.
(68) Andersen, J. B.; Frandsen, A. Absorption Efficiency of Receiving Antennas. *IEEE Trans. Antennas Propag.* **2005**, *53*, 2843−2849.
(69) Kwon, D.-H.; Pozar, D. M. Optimal Characteristics of an Arbitrary Receive Antenna. *IEEE Trans. Antennas Propag.* **2009**, *57*, 3720−3727.
(70) Fleury, R.; Soric, J.; Alù, A. Physical Bounds on Absorption and Scattering for Cloaked Sensors. *Phys. Rev. B: Condens. Matter Mater. Phys.* **2014**, *89*, 045122.
(71) Grigoriev, V.; Bonod, N.; Wenger, J.; Stout, B. Optimizing Nanoparticle Designs for Ideal Absorption of Light. *ACS Photonics* **2015**, *2*, 263−270.
(72) Miller, R. C. Optical Second Harmonic Generation in Piezoelectric Crystal. *Appl. Phys. Lett.* **1964**, *5*, 17−19.
(73) Linnenbank, H.; Linden, S. Second Harmonic Generation Spectroscopy on Second Harmonic Resonant Plasmonic Metamaterials. *Optica* **2015**, *2*, 698−701.
(74) Metzger, B.; Schumacher, T.; Hentschel, M.; Lippitz, M.; Giessen, H. Third Harmonic Generation in Complex Plasmonic Fano Structures. *ACS Photonics* **2014**, *1*, 471−476.
(75) Garrett, C.; Robinson, F. Miller's Phenomenological Rule for Computing Nonlinear Susceptibilities. *IEEE J. Quantum Electron.* **1966**, *2*, 328−329.
(76) Hentschel, M.; Utikal, T.; Giessen, H.; Lippitz, M. Quantitative Modeling of the Third Harmonic Emission Spectrum of Plasmonic Nanoantennas. *Nano Lett.* **2012**, *12*, 3778−3782.
(77) Butet, J.; Martin, O. J. F. Evaluation of the Nonlinear Response of Plasmonic Metasurfaces: Miller's Rule, Nonlinear Effective Susceptibility Method, and Full-Wave Computation. *J. Opt. Soc. Am. B* **2016**, *33*, A8−A15.
(78) Zuloaga, J.; Nordlander, P. On the Energy Shift between Near-Field and Far-Field Peak Intensities in Localized Plasmon Systems. *Nano Lett.* **2011**, *11*, 1280−1283.
(79) Luk'yanchuck, B.; Zheludev, N. I.; Maier, S. A.; Halas, N. J.; Nordlander, P.; Giessen, H.; Chong, C. T. The Fano Resonance in Plasmonic Nanostructures and Metamaterials. *Nat. Mater.* **2010**, *9*, 707−715.
(80) Miroshnichenko, A. E.; Flach, S.; Kivshar, Y. S. Fano Resonances in Nanoscale Structures. *Rev. Mod. Phys.* **2010**, *82*, 2257−2298.
(81) Zhang, S.; Genov, D. A.; Wang, Y.; Liu, M.; Zhang, X. Plasmon-Induced Transparency in Metamaterials. *Phys. Rev. Lett.* **2008**, *101*, 047401.
(82) Gallinet, B.; Martin, O. J. F. Ab-Initio Theory of Fano Resonances in Plasmonic Nanostructures and Metamaterials. *Phys. Rev. B: Condens. Matter Mater. Phys.* **2011**, *83*, 235427.
(83) Kern, A. M.; Martin, O. J. F. Surface Integral Formulation for 3D Simulation of Plasmonic and High Permittivity Nanostructures. *J. Opt. Soc. Am. A* **2009**, *26*, 732−740.
(84) Mäkitalo, J.; Suuriniemi, S.; Kauranen, M. Boundary Element Method for Surface Nonlinear Optics of Nanoparticles. *Opt. Express* **2011**, *19*, 23386−23399.
(85) Shen, S.; Meng, L.-Y.; Zhang, Y.; Han, J.; Ma, Z.; Hu, S.; He, Y.; Li, J.-F.; Ren, B.; Shih, T.-M. Plasmon-Enhanced Second-Harmonic Generation Nanorulers with Ultrahigh Sensitivities. *Nano Lett.* **2015**, *15*, 6716−6721.
(86) Sönnischen, C.; Franzl, T.; Wilk, T.; von Plessen, G.; Feldmann, J.; Wilson, O.; Mulvaney, P. Drastic Reduction of Plasmon Damping in Gold Nanorods. *Phys. Rev. Lett.* **2002**, *88*, 077402.
(87) Gallinet, B.; Martin, O. J. F. Refractive Index Sensing with Subradiant Modes: A Framework to Reduce Losses in Plasmonic Nanostructures. *ACS Nano* **2013**, *7*, 6978−6987.
(88) Wolf, D.; Schumacher, T.; Lippitz, M. Shaping the Nonlinear Near Field. *Nat. Commun.* **2016**, *7*, 10361.
(89) Biagioni, P.; Brida, D.; Huang, J.-S.; Kern, J.; Duò, L.; Hecht, B.; Finazzi, M.; Cerullo, G. Dynamics of Four-Photon Photoluminescence in Gold Nanoantennas. *Nano Lett.* **2012**, *12*, 2941−2947.
(90) Chen, W.-L.; Lin, F.-C.; Lee, Y.-Y.; Li, F.-C.; Chang, Y.-M.; Huang, J.-S. The Modulation Effect of Transverse, Antibonding, and Higher-Order Longitudinal Modes on the Two-Photon Photoluminescence of Gold Plasmonic Nanoantennas. *ACS Nano* **2014**, *8*, 9053−9062.

DOI: 10.1021/acsphotonics.6b00031
ACS Photonics 2016, 3, 1453−1460